J Comput Neurosci (2015) 38:129–142
DOI 10.1007/s10827-014-0531-7

Drift-diffusion simulation of the ephaptic effect in the triad synapse of the retina

Carl L. Gardner · Jeremiah R. Jones · Steven M. Baer · Sharon M. Crook

Received: 16 July 2013 / Revised: 28 August 2014 / Accepted: 12 September 2014 / Published online: 28 September 2014

Abstract Experimental evidence suggests the existence of a negative feedback pathway between horizontal cells and cone photoreceptors in the outer plexiform layer of the retina that modulates the flow of calcium ions into the synaptic terminals of cones. However, the underlying mechanism for this feedback is controversial and there are currently three competing hypotheses: the ephaptic hypothesis, the pH hypothesis, and the GABA hypothesis. The goal of this investigation is to demonstrate the ephaptic hypothesis by means of detailed numerical simulations. The drift-diffusion (Poisson-Nernst-Planck) model with membrane boundary current equations is applied to a realistic two-dimensional cross-section of the triad synapse in the goldfish retina to verify the existence of strictly electrical feedback, as predicted by the ephaptic hypothesis. The effect on electrical feedback from the behavior of the bipolar cell membrane potential is also explored. The computed steady-state cone calcium transmembrane current-voltage curves for several cases are presented and compared with experimental data on goldfish. The results provide convincing evidence that an ephaptic mechanism can produce the feedback effect seen in experiments. The model and numerical methods presented here can be applied to any neuronal circuit where dendritic spines are invaginated in presynaptic terminals or boutons.

Keywords Synapse · Retina · Ephaptic effect · Drift-diffusion model

Action Editor: Mark van Rossum

C. L. Gardner (✉) · J. R. Jones · S. M. Baer · S. M. Crook
School of Mathematical & Statistical Sciences,
Arizona State University, Tempe AZ 85287, USA
e-mail: carl.gardner@asu.edu

1 Introduction

The amount of visual processing that occurs in the retina before the signal reaches the visual cortex is often underestimated. Various feedback networks are known to exist within the retina, from the outer plexiform layer to the neuropil of the inner plexiform layer. To unravel how visual processing takes place in the retina it is essential to understand how these feedback mechanisms work. The most well-studied feedback is in the triad synapse in the outer plexiform layer (OPL) where rods, cones, bipolar, and horizontal cells interact. We have shown in a previous study (Gardner et al. 2013) how the geometric configuration of these cells gives rise to an ephaptic feedback response, using a vastly simplified rectangular geometry for the intersynaptic space. Here we demonstrate the ephaptic hypothesis by means of detailed numerical simulations in a realistic two-dimensional cross-section of the goldfish triad synapse using the drift-diffusion (Poisson-Nernst-Planck) model plus membrane boundary current equations.

In the outer plexiform layer of the retina, the synaptic terminals of rods and cones form synapses with two other neuron types: horizontal cells and bipolar cells. The bipolar cells carry visual information to the inner plexiform layer and the horizontal cells form a network connected through gap junctions that is confined to the OPL. Photoreceptors translate visual information into electric currents through changes in their membrane potentials. Horizontal cells in turn respond to these changes, providing the input to bipolar cells. The horizontal cell feedback to the cones may be viewed as a signal processing mechanism that removes low spatial and temporal frequencies to regulate release of glutamate by cones. In this investigation, we will consider a particular type of synapse in the OPL formed by a cone,

a horizontal cell, and a bipolar cell, referred to as a triad synapse.

The synaptic terminal of a cone—the cone pedicle—forms a cavity-like structure with a highly convoluted geometry. The pedicle is invaginated by multiple spines extending from the dendrites of horizontal cells and bipolar cells. A triad synapse is a synapse in which a bipolar cell, flanked by two or more horizontal cells, comes into close proximity with the cone pedicle. In a typical goldfish cone pedicle, there are on average 5–16 triad synapses (Kamermans and Fahrenfort 2004). An idealized diagram of a two dimensional slice of a triad synapse is shown in Fig. 1. Note that we are modeling only calcium channels (along the thick red curve on the cone pedicle membrane) and hemichannels (along the thick dark blue curve on the horizontal cell membrane). The calcium transmembrane current flows into the cone for the applied voltages of interest here, while the hemichannel transmembrane current can flow into or out of the horizontal cell. A simple equivalent circuit model is given in Fig. 3 of Kamermans and Fahrenfort (2004).

Neurotransmission in the triad synapse is modulated by the flow of calcium ions through the cone pedicle membrane. The area inside the cone pedicle directly across from the bipolar cell contains vesicles that release the neurotransmitter glutamate. The rate at which glutamate is being released from the cone increases with the cone's intracellular calcium level.

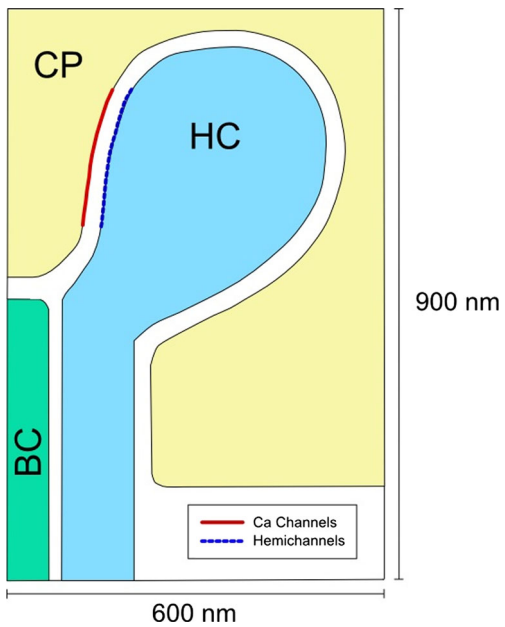

Fig. 1 Diagram of the triad synapse and physical locations of the calcium channels and hemichannels (CP = cone pedicle, HC = horizontal cell, and BC = bipolar cell). Lengths are in nm

We apply our model to the experiments performed by Verweij et al. (1996) on goldfish retinas. In their experimental setup, an isolated goldfish retina is saturated with a 65 μm bright spot of red light. The spot is a constant (non-flickering) test region in the presence and absence of a full-field background illumination. The spot stimulates the cone and the background illumination stimulates the rods, which have gap junctions with the cones. The horizontal cells have synapses with the cones (but not directly with the rods). The calcium current through the cone membrane is then measured with and without background illumination using patch clamp techniques with a Ringer's solution designed to block the currents contributed by other ions.

In the absence of background illumination, cones depolarize, activating voltage-gated calcium channels in the cone and thereby increasing the cone's intracellular calcium levels. This increase in turn triggers the cone membrane to release more glutamate, which diffuses across the synaptic cleft and binds to receptor sites on the horizontal cell. The binding of glutamate activates cation-specific channels in the horizontal cell, resulting in an inward current and depolarization of the postsynaptic membrane. On the other hand, when illuminated the cone hyperpolarizes, leading to a reduction in glutamate release. This reduction causes fewer glutamate-gated channels in the horizontal cell to open and therefore less current enters the horizontal cell, leading to a hyperpolarization of the horizontal cell membrane.

It has been observed that when horizontal cells become hyperpolarized the net result is an increase in intracellular cone calcium levels, increasing glutamate release and bringing the horizontal cell back to its resting state, implying a negative feedback pathway from horizontal cells to cones (Kamermans and Fahrenfort 2004). The existence of this feedback pathway is irrefutable (Byzov and Shura-Bura 1986; Verweij et al. 1996) although the underlying mechanism has been a subject of heated debate for over twenty years.

There are three competing hypotheses regarding the feedback mechanisms: the ephaptic hypothesis, the pH hypothesis, and the GABA hypothesis. Experimental evidence exists throughout the literature that both supports and contradicts these three hypotheses, making it difficult to draw any significant conclusions. The most recent research in this area suggests that the ephaptic and pH effects are both present but operate on different time scales (M. Kamermans, private communication).

The goal of this investigation is to demonstrate the ephaptic hypothesis through numerical simulations of the microscopic drift-diffusion model with membrane boundary current equations. This model is applied to a realistic two-dimensional cross-section of the triad synapse

in the goldfish retina to verify the existence of strictly electrical feedback, as predicted by the ephaptic hypothesis, reproducing the shift in the experimental background on/off cone calcium transmembrane current-voltage curve ("calcium IV curve" for short) in Fig. 8 from a microscopic, electro-diffusion viewpoint.

The prediction of the shift in the calcium IV curve proves the ephaptic hypothesis in the context of a microscopic model. Only the unshifted curve without background illumination is calibrated by adjusting the four parameters in the calcium channel model (13) *within a physiologically relevant range. Then the drift-diffusion model, with no further adjustment, gives the correctly shifted IV curve with background illumination, proving the ephaptic hypothesis.*

1.1 The Ephaptic Hypothesis

The ephaptic hypothesis was first proposed in 1986 by Byzov and Shura-Bura (1986) and has since been repeatedly tested and modified. In short, the ephaptic hypothesis claims that the negative feedback pathway from horizontal cells to cones is electrical in nature. The specialized geometry of the triad synapse contains narrow extracellular regions between horizontal cells and the cone pedicle which have a relatively large resistivity. Ionic current passing from these high-resistance regions into the horizontal cell via ionic channels causes the extracellular potential in the cleft to become more negative. The increased difference in the cone membrane potential in turn activates calcium channels. Horizontal cell hyperpolarization under background illumination activates inward currents enhancing the cone membrane depolarization, which ultimately leads to an increase in intracellular calcium levels in the cone. In a voltage clamp experiment, this increase in cone calcium levels under background illumination is seen as a shift in the calcium IV curve to more negative potentials.

This mechanism depends on active channels in the horizontal cell membrane that are responsible for the inward current. Byzov originally proposed the glutamate-gated channels at the tips of the horizontal cell as a candidate for this mechanism (Byzov and Shura-Bura 1986). However, this idea was discarded when Kamermans and Spekreijse (1999) tested it in goldfish using dinitroquinoxaline (DNQX), a glutamate antagonist, to block the transmembrane current through the glutamate-gated channels. The results showed no change in the shift in the calcium IV curve. Instead of abandoning the ephaptic hypothesis, Kamermans and colleagues instead modified it by proposing that hemichannels in the tips of the horizontal cells were responsible for the inward current. Hemichannels are often considered as one-way gap junctions, in the sense that they connect the interior of a cell to the extracellular space with no voltage- or ligand-gating mechanism. This idea wa driven by physiological studies that confirmed that such channels are indeed located on the horizontal cell and are in close proximity with the calcium channels and glutamate release sites (Janssen-Beinhold et al. 2001). The modified hypothesis has gained momentum in recent years due to the successful experiments designed to test it. In one experiment, Kamermans and colleagues performed identical voltage clamp experiments on two groups of zebrafish: a genetically modified group that lacked the codons necessary to specify the hemichannel proteins and an unmodified control group (Klaassen et al. 2011). The results showed that the calcium IV curves in the modified subjects were not shifted, while the curves for the control group were shifted, a clear indication that the feedback is indeed dependent on hemichannels.

Although the ephaptic hypothesis has enjoyed some experimental success, it continues to be controversial. Dmitriev and Mangel (2006) employed a circuit model to argue that the resistance of the extracellular cleft must be extremely large to induce the observed feedback and that such an extreme resistance value is not physically reasonable. However, the external resistivity is modeled successfully in Gardner et al. (2013), where it is shown that the drift-diffusion model creates the correct resistances for the ephaptic effect in the intersynaptic space along the sides of the horizontal cell spine.

In addition, the other two hypotheses have received some experimental support.

1.2 The pH Hypothesis

The pH hypothesis proposes that feedback is modulated by changes in extracellular proton concentrations. According to this hypothesis, hyperpolarization of horizontal cells alkalinizes the extracellular space which serves to alter the gating mechanism of pH-sensitive calcium channels in the cone membrane (Barnes et al. 1993; Hirasawa and Kaneko 2003). However, the mechanism by which horizontal cell polarization controls extracellular pH levels is still unknown, although researchers have proposed many possible candidates (Kamermans and Fahrenfort 2004; Vessey et al. 2005; Bouvier et al. 1992; Hirasawa and Kaneko 2003).

The pH hypothesis has a fair amount of experimental support. It has been shown that extracellular pH levels can affect voltage-sensitive calcium channels (DeVries 2001; Prodhom et al. 1987). Further, experiments with goldfish, tiger salamanders, and macaque monkeys have shown that inhibition of extracellular pH fluctuations, induced by

inserting high concentrations of artificial pH buffers, can greatly affect the feedback responses (Babai and Thoreson 2009; Cadetti and Thoreson 2006; Davenport et al. 2008; Hirasawa and Kaneko 2003; Vessey et al. 2005).

The validity of this hypothesis has also been questioned. One study on the goldfish retina showed that feedback responses were not altered in the presence of high concentration of HEPES, an artificial pH buffer (Mangel et al. 1985; Kamermans and Fahrenfort 2004). It has also been argued that the experimental techniques used to test the hypothesis can have unintended side effects that would affect other feedback mechanisms (Fahrenfort et al. 2009). For example, the insertion of pH buffers can cause acidification of the intracellular horizontal cell solution, which can inhibit hemichannel activity. Since the presence of pH affects most biological processes, on varying time scales from milliseconds to hours, it is difficult to prove experimental support for a specific pH effect.

1.3 The GABA Hypothesis

The GABA hypothesis asserts that feedback is modulated by a chemical neurotransmitter with γ-aminobutyric acid (GABA) being the primary candidate (Dunlap and Fischbach 1981; Gerschenfeld et al. 1980; Nelson et al. 1990; Piccolino 1995). The theory claims that horizontal cells constantly release GABA which diffuses across the extracellular space, binding to the cone membrane, inhibiting calcium channels. Under background illumination induced hyperpolarization of the horizontal cell, the quantity of GABA released by the horizontal cell is reduced, allowing more calcium to flow into the cone.

The GABA hypothesis has received some experimental support. A GABA synthesizing enzyme, known as glutamic acid decarboxylase (GAD), has been found to exist in some horizontal cells of certain animals (Chun and Wässle 1989; Guo et al. 2010; Johnson and Vardi 1998; Lam et al. 1979; Vardi et al. 1994). It has also been observed that GABA release sites on horizontal cells act in a manner consistent with the hypothesis, i.e., they are inhibited by hyperpolarization (Ayoub and Lam 1985; Marc et al. 1978; Schwartz 1982; 1987). Most importantly, several pharmacological studies of the catfish and carp retina have revealed that application of GABA antagonists does indeed affect feedback under background illumination (Lam et al. 1978; Murakami et al. 1982a, b).

Most opposition to the GABA hypothesis stems from the fact that Kamermans' experiments were able to alter feedback responses in a GABA independent manner. It is most likely that GABA does play some role in the overall process but only in certain instances and for certain species. However, it seems clear that in the goldfish retina the feedback is not dominated by a GABA-ergic mechanism.

1.4 Summary of Scientific Results

This investigation examines the ephaptic hypothesis by means of numerical simulations of the goldfish triad synapse at a microscopic level using the drift-diffusion model with membrane boundary current equations.

The drift-diffusion code is a general purpose membrane/ionic bath simulator, and has already been applied to the potassium channel in Gardner and Jones (2011), and to membrane currents between heart muscle cells, in addition to the retina problem. The drift-diffusion model, as applied to the triad synapse, is calibrated in Gardner et al. (2013) to reproduce, in a simplified geometry, the experimental calcium IV curves.

The main result of this investigation is verification of the ephaptic hypothesis by reproducing the experimental *shifted* background on/off calcium IV curves from a microscopic, electro-diffusion simulation with only four parameters (all in the calcium channel current model in equation (13)), with the background illumination turned on and off by adjusting the intracellular potential of the horizontal cell at the bottom of the computational region. The experimental background on/off calcium IV curves can be reproduced in a simpler compartment model (Fahrenfort et al. 2009), but here we derive this result from a local microscopic model. We also predict that there are 50 % ON and 50 % OFF type bipolar cells in the triad synapses (see Fig. 8).

Related simulations in a vastly simplified rectangular geometry—using an extra parameter in the calcium channel current model to implement turning the background illumination on and off—supporting the ephaptic mechanism are presented in Gardner et al. (2013); there we showed that the strength of the feedback response depends on the geometric configuration of the postsynaptic processes within the triad synapse.

Baer et al. (to appear) discuss the primary importance of the ephaptic effect vs. the effect of GABA on *time-dependent* simulations of calcium current responses of the cat retina to steady and flickering test stimuli with illuminated or unilluminated background, in the context of a multi-scale *macroscopic* two-dimensional model. In vertebrate outer retina, changes in the membrane potential of horizontal cells affect the calcium influx and glutamate release of cone photoreceptors via a negative feedback mechanism. This feedback has a number of important physiological consequences. One is called background-induced flicker enhancement in which the onset of dim background enhances the center flicker response of horizontal cells. This model, a partial differential equation system, incorporates both the GABA and ephaptic feedback mechanisms on the scale of an individual synapse and the scale of the receptive field. Simulation results, in comparison with experiments, indicate that the ephaptic mechanism is dominant in

reproducing the major temporal dynamics of background-induced flicker enhancement.

2 Drift-Diffusion Equations

To model the potential and the ionic currents in the triad synapse of the retina, and to compute the Ca^{2+} currents into the cone pedicle, we will use the drift-diffusion model. The discrete distribution of ions is described by continuum ion densities $n_i(\mathbf{x}, t)$ for $i = Ca^{2+}$, Na^+, K^+, and Cl^-, and the positive and negative ions flow in water in an electric field $\mathbf{E}(\mathbf{x}, t)$. The drift-diffusion model is derivable from the Boltzmann transport equation plus Poisson's equation; thus additional forces and flows can be incorporated into the model if experimentally observed. In the experimental setup, a voltage bias is applied between the cone and the horizontal cell by means of a patch clamp.

Consider a region such as that shown in the two dimensional slice of the triad synapse in Fig. 1. This region can be separated into four compartments: cone interior, horizontal cell (HC) interior, bipolar cell (BC) interior, and extracellular. Each compartment is assumed to be filled with a salt solution containing the four common biological ions Ca^{2+}, Na^+, K^+, and Cl^-, which we treat as continuous charge, rather than individual ions. This continuum model has been used successfully in many biological applications (Eisenberg et al. 1995; Nonner and Eisenberg 1995; Gardner et al. 2004; Gardner et al. 2013).

The presence of dissociated ions in a salt bath induces a potential field, which in turn affects the flow of ions. To model the evolution of the ion densities and the electric potential, we utilize a system of partial differential equations known as the drift-diffusion or Poisson-Nernst-Planck equations that hold in the various compartments. Treatment of the state variables on the membranes and boundaries will be discussed below. We neglect water flow effects in this investigation; these effects (Eisenberg et al. 2010; Mori et al. 2011) will be included in future work unless experimental work demonstrates that osmotically induced flows have no effect.

By requiring conservation of charge for each ionic species, we obtain the continuity equation

$$\frac{\partial n_i}{\partial t} + \nabla \cdot \mathbf{f}_i = 0, \tag{1}$$

where $i = Ca^{2+}$, Na^+, K^+, and Cl^-, and where $\mathbf{f}_i$ is the flux of the ith ionic species. Gauss' Law relates the ion densities to the electric potential ϕ:

$$\nabla \cdot (\epsilon \nabla \phi) = -\rho = -\sum_i q_i n_i, \quad \mathbf{E} = -\nabla \phi, \tag{2}$$

where ϵ is the dielectric coefficient of water, ρ is the total charge density, and q_i is the ionic charge of species i. The ionic flux has drift and diffusion terms

$$\mathbf{f}_i = z_i \mu_i n_i \mathbf{E} - D_i \nabla n_i, \tag{3}$$

where $z_i = q_i/e$, D_i is the diffusion coefficient, and μ_i the mobility coefficient of ionic species i. The diffusion and mobility coefficients satisfy the Einstein relation $D_i = \mu_i k_B T/e$ where k_B is the Boltzmann constant, T is the absolute temperature of the medium, and $e > 0$ is the unit charge. For most biological applications, $T \approx 310$ K, a typical body temperature, so $k_B T \approx 1/40$ eV. The ionic flux $\mathbf{f}_i$ for each ionic species can be converted into electric current densities $\mathbf{j}_i$ via the simple relation

$$\mathbf{j}_i = q_i \mathbf{f}_i \tag{4}$$

and the total current density $\mathbf{j}$ is

$$\mathbf{j} = \sum_i \mathbf{j}_i \,. \tag{5}$$

In general, the parameters D_i, μ_i, and ϵ can be treated as functions of space. For our purposes, it is reasonable to assume that these parameters are constant in the physical domain of the problem. The constant values used for the parameters are shown in Table 1. To summarize, the drift-diffusion model reduces to the system

$$\frac{\partial n_i}{\partial t} = D_i \nabla^2 n_i + z_i \mu_i \nabla \cdot (n \nabla \phi) \tag{6}$$

$$\nabla^2 \phi = -\frac{1}{\epsilon} \sum_i q_i n_i \,. \tag{7}$$

This model forms a nonlinear parabolic/elliptic system of $N_{species} + 1$ partial differential equations where $N_{species}$ is the number of ionic species included in the model. The state variables of the model are n_i and ϕ, which have Dirichlet and/or Neumann boundary conditions.

It is known experimentally that the ion densities in biological fluids remain at constant values when far away from cell membranes. The values of these constant ion densities

Table 1 Physical parameters used in the drift-diffusion equations

Parameter	Value	Description
D_{Ca}	0.8 nm^2/ns	diffusion coefficient of Ca^{2+}
D_{Cl}	2 nm^2/ns	diffusion coefficient of Cl^-
D_{Na}	1.3 nm^2/ns	diffusion coefficient of Na^+
D_K	2 nm^2/ns	diffusion coefficient of K^+
μ_{Ca}	32 nm^2/(V ns)	mobility coefficient of Ca^{2+}
μ_{Cl}	80 nm^2/(V ns)	mobility coefficient of Cl^-
μ_{Na}	52 nm^2/(V ns)	mobility coefficient of Na^+
μ_K	80 nm^2/(V ns)	mobility coefficient of K^+
ϵ	80	dielectric coefficient of water

n_{bi} are referred to as the bath densities and have been measured for several cases. For any given ionic species, the bath densities can be very different depending on whether the region is inside a cell or outside a cell. For example, a typical intracellular bath density for calcium in a mammalian organism is $n_{b,Ca} = 10^{-4}$ mM, while a typical extracellular bath density is $n_{b,Ca} = 2$ mM. It is also known that biological fluids maintain charge neutrality away from membranes. To ensure this, we must enforce the condition

$$\sum_i q_i n_{bi} = 0. \tag{8}$$

However, the experimentally measured values of the four common ionic species do not generally satisfy this relation since there are a number of other charged molecules that contribute. To get around this, we use the typical bath densities for the positive ions and treat chloride as the general negative charge carrier, setting

$$n_{b,Cl} = \sum_{i \neq Cl} z_i n_{bi} \,. \tag{9}$$

The values for the bath densities are shown in Table 2. Note that the values for $n_{b,Cl}$ are not typical and have been adjusted to ensure charge neutrality.

The primary fluid dynamics is determined in each intracellular or extracellular region by the dominant ions (see Table 2), with a total density in each case of approximately 300 mM = 1.8×10^{20} ions/cm^3 = 1.8×10^8 ions/μm^3 (1 mM = 6.022×10^{17} ions/cm^3), typical of electron and hole densities in semiconductor devices, where the drift-diffusion model is known to give excellent results for 1 μm devices. There may be some stochastic effects in the calcium currents, but the experimental data are not yet accurate enough to see such effects.

2.1 External Boundary Conditions

On the external computational boundaries we use a mixture of Dirichlet and Neumann boundary conditions. The most natural boundary condition to use for the ion densities is the Dirichlet condition $n_i = n_{bi}$, since it is reasonable to assume the ion densities remain at their bath values away from membranes. Along the y axis of symmetry (see Fig. 1), we use the homogeneous Neumann boundary condition $\mathbf{n} \cdot \nabla n_i = 0$, where $\mathbf{n}$ is the outward pointing unit normal vector to the boundary.

Table 2 Values of the intracellular and extracellular bath densities for the four common biological ions used in the simulations

Ion	Intracellular	Extracellular
Ca^{2+}	10^{-4} mM	2 mM
Cl^-	160 mM	146.5 mM
Na^+	10 mM	140 mM
K^+	150 mM	2.5 mM

The boundary conditions for ϕ are chosen in a way that attempts to mimic the voltage clamp experiment. In such an experiment, micro-electrodes that are held at fixed potentials are inserted at specific locations, usually one inside the cone and the other "ground" electrode far away from the cone. Along the top of the cone pedicle, U_{CP} is set to V_{clamp}, where V_{clamp} is the clamped potential, or holding potential, with respect to ground.

Figure 2 gives the boundary conditions on the electrostatic potential along the outer boundary of the computational domain. The specifications of the Dirichlet boundary values for the holding potential U_{CP} and for the intracellular potentials U_{BC} and U_{HC} are given in Section 3. U_{ref} denotes a fixed reference potential, which is not the absolute physical ground $\phi = 0$ since that is far away from the computational region, but is taken to be $U_{ref} = -40$ mV, which equals U_{HC}^{off} with background illumination off. The applied voltage across the triad synapse is $U_{CP} - U_{ref}$. A homogeneous Neumann boundary condition on the normal derivative $\mathbf{n} \cdot \nabla\phi = 0$ is imposed on the remainder of the outer boundary.

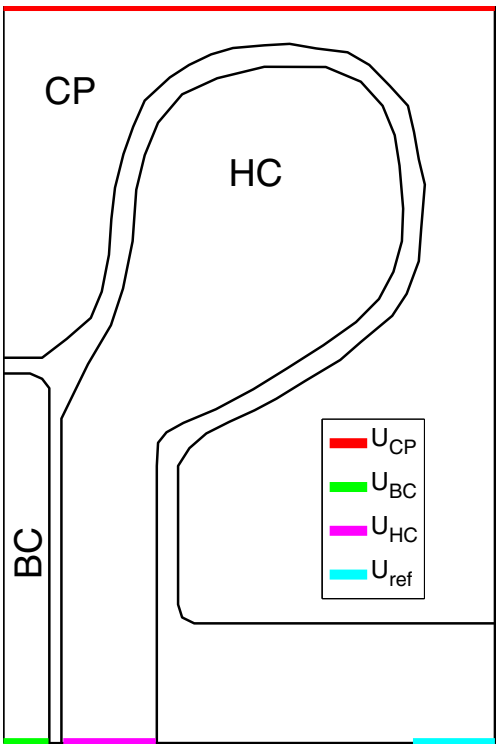

Fig. 2 Boundary conditions on the electrostatic potential along the outer boundary of the computational domain. U_{CP}, U_{BC}, and U_{HC} are specified potentials, where CP = cone pedicle, BC = bipolar cell, and HC = horizontal cell. U_{ref} denotes a fixed reference potential. The applied voltage across the triad synapse is $U_{CP} - U_{ref}$. A homogeneous Neumann boundary condition on the potential is imposed on the remainder of the outer boundary

The cone pedicle, horizontal cell, and bipolar cell are not isopotential (see Barcilon et al. (1971) for nerve cells). The potential at the top boundary of the cone pedicle (see Fig. 2) is held at a fixed voltage U_{CP} (Dirichlet boundary condition), while the sides of the cone pedicle obey a homogeneous Neumann boundary condition on the potential. We believe that these are physically relevant boundary conditions reflecting the fact that the electrode within the cone is very far "above" the computational region, and that the voltage contours will therefore be approximately horizontal lines near the top of the cone pedicle in the computational region. The homogeneous Neumann boundary conditions at the sides of the computational region mathematically represent a coupling to a reservoir at either side, extending the cone pedicle to the left and right. In fact, the homogeneous Neumann boundary condition on the densities as well as the potential at the left boundary makes it an axis of symmetry. At the right boundary, the Dirichlet boundary conditions on densities represent a coupling to an infinite reservoir bath. There must be a voltage gradient within the cone pedicle, as well as within the horizontal cell and bipolar cell, as the voltage far "above" the cone terminal falls toward ground far "below" the computational region.

Large potential gradients do appear within the cone pedicle and horizontal cell, as a consequence of the potential differences applied across them in the boundary conditions, which approximate the voltage clamp experimental setup. The largest potential gradients actually occur across the capacitative cell membranes (see Figs. 3, 4, 5 and 6), but with an applied voltage of $U_{CP} - U_{ref}$ (see Fig. 2) in the range of $[-40, 50]$ mV across the vertical domain of $0.9\,\mu$m, large potential gradients must appear within the cone pedicle and horizontal cell except when the applied voltage is small ($|U_{CP} - U_{ref}| \ll 5$ mV).

The 2D cross-section that we have chosen is reflected about the vertical axis at the left boundary by our boundary conditions (homogeneous Neumann boundary conditions on the densities and the potential) to produce a good approximation to the 3D problem, which has one bipolar cell and two horizontal cell spines per triad synapse (the cone pedicle has on average 20 triad synapses). The additional 3D effects would generate only small corrections to the calcium IV curves, yet the computational times would be prohibitive for exploring the parameter space of the model. The calcium IV curves computed with the 2D model agree with the experimental calcium IV curves mainly to within 10 %, and everywhere to within 20 %. Complete agreement is not to be expected because of the theoretical argument presented by Klaassen et al. (2011) that the shift in the calcium IV curve under background illumination is a pure translation, and that extraneous effects may have distorted the experimental shift data in Verweij et al. (1996) (see further discussion below in Section 3).

In future work we will extend the triad synapse simulation region in Fig. 1 both "vertically" and "horizontally" to include arrays of triad synapses. This extension of the computational region in the 2D cross-sectional plane is much more important physically than any 3D effects.

2.2 Membrane Boundary Conditions

Biological fluids maintain charge neutrality away from membranes, though charge layers can accumulate on membranes, violating the local neutrality. To resolve the charge

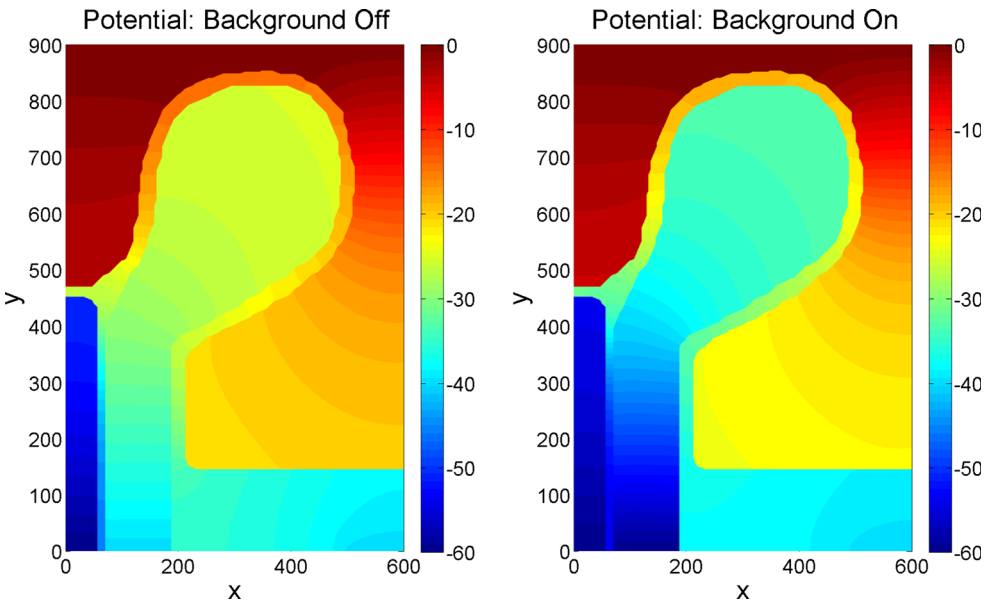

Fig. 3 Steady-state potential in the synapse with $U_{CP} = 0$ mV, $U_{BC} = -60$ mV, $U_{HC}^{off} = -40$ mV, and $U_{HC}^{on} = -60$ mV. Lengths are in nm and the potential is in mV

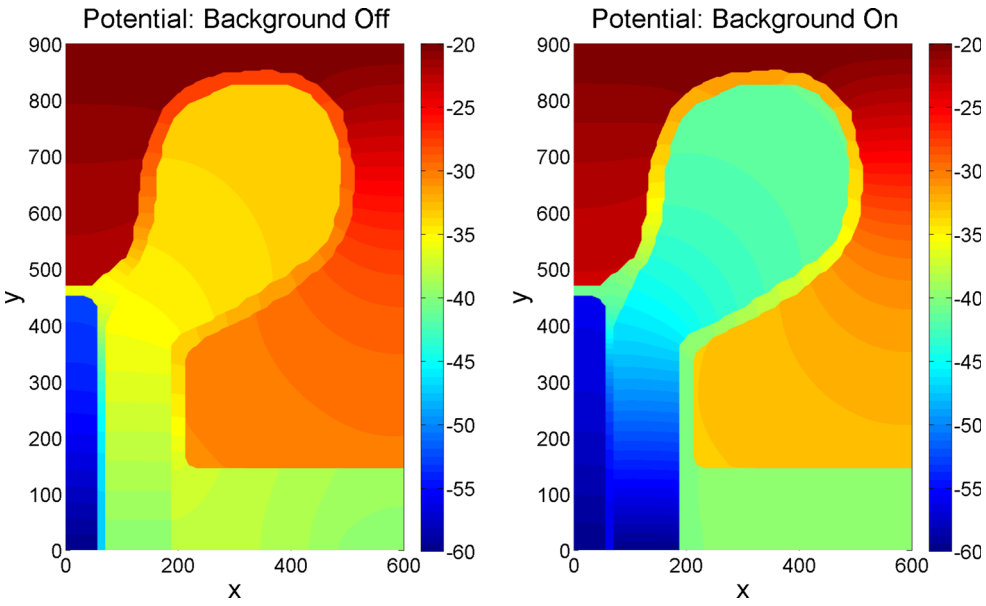

Fig. 4 Steady-state potential in the synapse with $U_{CP} = -20$ mV, $U_{BC} = -60$ mV, $U_{HC}^{off} = -40$ mV, and $U_{HC}^{on} = -60$ mV. Lengths are in nm and the potential is in mV

layers, we must develop a model for the membrane surface charge densities. Our approach to modeling the membrane follows that of Mori et al. (2007) and Mori and Peskin (2009). However, in their treatment, they use asymptotic expansions with intermediate matching to avoid dealing with charge layers, while we actually resolve these layers.

The main idea is to treat the membrane as a double-valued sheet in three dimensions. We label the sides of the membranes as + (intracellular) and − (extracellular). The membrane is modeled as a capacitor with zero thickness in which ions can accumulate on and/or pass through either side, resulting in surface charge densities $\sigma_i^{\pm}$, where i indexes the four ionic species and the $\pm$ superscript indicates the side of the membrane. The state variables of the drift-diffusion model, n_i and ϕ, are also defined on the membrane and are double-valued, denoted as $n_i^{\pm}$ and $\phi^{\pm}$, respectively. To obtain the membrane boundary conditions for the ion densities, we relate the spatial charge densities $n_i^{\pm}$ to the surface charge densities $\sigma_i^{\pm}$:

$$\sigma_i^{\pm} = q_i l_D^{\pm} \left(n_i^{\pm} - n_{bi}^{\pm} \right), \tag{10}$$

where $n_i^{\pm}$ is the ion density on the membrane, and where

$$l_D^{\pm} = \sqrt{\frac{\epsilon k_B T}{\sum_i q_i^2 n_{bi}^{\pm}}} \tag{11}$$

is the Debye length, which is typically around 1 nm for biological baths. Indeed, using the parameter values from

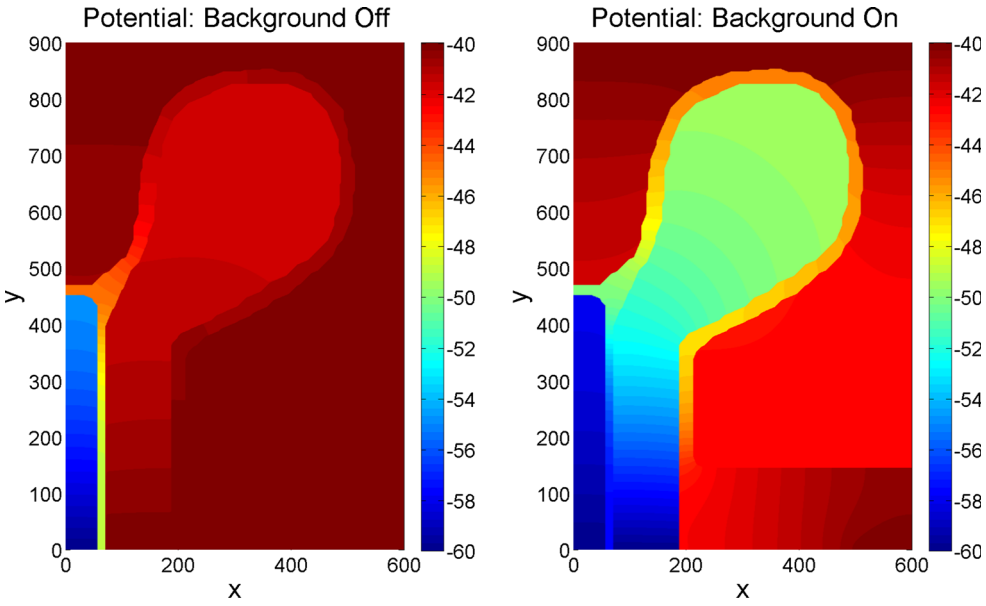

Fig. 5 Steady-state potential in the synapse with $U_{CP} = -40$ mV, $U_{BC} = -60$ mV, $U_{HC}^{off} = -40$ mV, and $U_{HC}^{on} = -60$ mV. Lengths are in nm and the potential is in mV

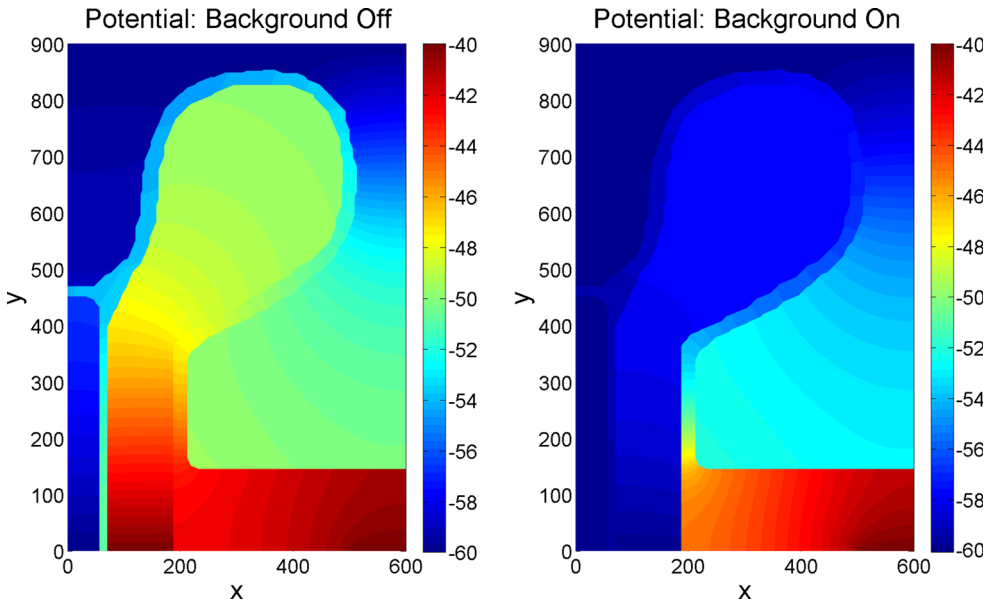

Fig. 6 Steady-state potential in the synapse with $U_{CP} = -60$ mV, $U_{BC} = -60$ mV, $U_{HC}^{off} = -40$ mV, and $U_{HC}^{on} = -60$ mV. Lengths are in nm and the potential is in mV

Tables 1 and 2, we have that $l_D^+ \approx 0.78$ nm and $l_D^- \approx 0.79$ nm.

Assuming that the total charge on the membrane is overall neutral, the ion densities on the membranes must satisfy equation (1). Using this fact and the definition of electric current density in equation (4), we have

$$\frac{\partial \sigma_i^{\pm}}{\partial t} = -l_D^{\pm} \nabla \cdot \mathbf{j}_i^{\pm} \mp j_{m,i}, \tag{12}$$

where $j_{m,i}$ is the transmembrane current. Note that we are using the sign convention for $j_{m,i}$ in which current flowing into a cell is negative and current flowing out of a cell is positive.

For the triad synapse, we model the two channel types in specific locations (see Fig. 1) on the membranes which are important to ephaptic feedback: voltage-gated calcium channels in the cone pedicle membrane and hemichannels in the horizontal cell membrane (Kamermans et al. 2001; Kamermans and Fahrenfort 2004).

We model the channel locations on the membranes as a continuum of channels with a uniform density. The calcium channels in the cone pedicle (CP) have been experimentally shown to obey a nonlinear Ohm's law with a voltage dependent conductance function (Kamermans et al. 2001), which we use in our model:

$$j_{m,Ca} = \frac{g_{Ca,CP}(V_m - E_{Ca,CP})}{N_s A_m [1 + \exp\{(\theta - V_m)/\lambda\}]}, \tag{13}$$

where $V_m = \phi^+ - \phi^-$ is the membrane potential, $g_{Ca,CP}$ is the maximum calcium conductance, $E_{Ca,CP}$ is the reversal potential of calcium, N_s is the average number of calcium channel sites in a cone pedicle, A_m is the surface area of the section of the cone pedicle containing calcium channels, θ is the half-activation potential, and λ is a curve fitting parameter. The normalization factors N_s and A_m require some explanation. Equation (13) is motivated by experimental data, which measure actual currents instead of current densities. Further, the experiments measure the total current through a given cone pedicle, which contains many triad synapses. On average, each pedicle has about $N_s = 20$ calcium channel sites. In addition, the area A_m of the region of the cone pedicle containing calcium channels is estimated to be about 0.1 μm^2. Thus dividing the current by A_m converts it into a current density and dividing by N_s gives the average current density over a given channel site.

The effects of the hyperpolarization of the horizontal cell on the cone calcium transmembrane current are modeled at a strictly local, microscopic level through the local values of the electric potential, but the local values of the electric potential change in response to a change in the boundary condition U_{HC} under background illumination.

The hemichannels in the horizontal cell are believed to be non-specific cation channels (Kamermans and Fahrenfort 2004) and thus we allow all cations to pass through them. The current-voltage relationship for hemichannels is experimentally observed to be linear, with an overall reversal potential of zero and a constant conductance of g_{hemi} (Klaassen et al. 2011). However, this includes the current from all cations and does not give any information about individual ionic currents. A reasonable approach is then to model each current density with a linear Ohm's law:

$$j_{m,i} = g_i(V_m - E_i)/(N_s A_m) \tag{14}$$

and impose the constraints

$$\sum_i g_i = g_{hemi} \tag{15}$$

Table 3 Hemichannel and other membrane parameters based on experimental estimations

Parameter	Value	Description
E_{Ca}	50 mV	reversal potential of Ca^{2+}
E_{Na}	50 mV	reversal potential of Na^{+}
E_K	−60 mV	reversal potential of K^{+}
g_{Ca}	1.5 nS	conductance of Ca^{2+} current
g_{Na}	1.5 nS	conductance of Na^{+} current
g_K	2.5 nS	conductance of K^{+} current
g_{hemi}	5.5 nS	total hemichannel conductance
C_m	1 μF/cm^2	capacitance per area
A_m	0.1 μm^2	HC spine head area
N_s	20	number of HC spines per synapse

and

$$\sum_i g_i E_i = 0 \tag{16}$$

to guarantee consistency with the experimental data. The hemichannel parameters are shown in Table 3. The calcium channel parameters are shown in Table 4.

The location of the calcium channels in the cone membrane and the hemichannels on the horizontal cell membrane are not arbitrary and in fact are located in such a way as to enable ephaptic communication. Figure 1 shows the regions in which experimentalists believe the channels are located (Kamermans and Fahrenfort 2004), which we also use in our model. In order to be able to compare our results to empirical data, we must approximate the current though an entire cone pedicle. To do this, we first compute the average current density over the channel region via the trapezoidal rule for numerical integration and then multiply the result by the normalization factors N_s and A_m. Thus the calcium transmembrane current for an entire cone pedicle is approximated as

$$I_{Ca} = \frac{N_s A_m}{\ell_C} \int_C j_{m,Ca}\, ds, \tag{17}$$

where C is the segment of the membrane containing the calcium channels and ℓ_C is the arc length of C.

The membrane boundary conditions for the state variables on the membrane are determined in the following way:

Table 4 Calcium channel parameters for equation (13) used in the simulations

Parameter	Value	Description
$g_{Ca,CP}$	2.2 nS	maximum conductance of calcium channels
$E_{Ca,CP}$	50 mV	reversal potential of calcium
λ	3 mV	kinetic parameter
θ	5 mV	half-activation potential

assuming we have solved equation (12) at the given time, we can use equation (10) to obtain the boundary conditions for $n_i^{\pm}$. Solving for $n_i^{\pm}$ gives

$$n_i^{\pm} = n_{bi}^{\pm} + \frac{\sigma_i^{\pm}}{q_i l_D^{\pm}}. \tag{18}$$

One of the boundary conditions for ϕ on the membranes can be determined by treating the membrane as a capacitor with a surface charge density σ and capacitance per unit area C_m, resulting in the jump condition

$$[\phi] \equiv \phi^{+} - \phi^{-} = \frac{\sigma}{C_m}, \tag{19}$$

where σ is defined as

$$\sigma = \sum_i \sigma_i^{+} = -\sum_i \sigma_i^{-}. \tag{20}$$

This definition assumes the membrane remains charge neutral, yielding a second jump condition:

$$[\mathbf{n}_m \cdot \nabla\phi] \equiv \mathbf{n}_m \cdot \nabla\phi^{+} - \mathbf{n}_m \cdot \nabla\phi^{-} = 0, \tag{21}$$

where $\mathbf{n}_m$ is the unit normal vector of the membrane pointing from the − side to the + side. In other words, the normal component of the electric field is continuous across the membrane.

Lipid membranes and ionic channels usually have permanent "built-in" charges independent of the electric potential, which are functions of pH and calcium concentration. These charge distributions can be incorporated (see Eisenberg 1996) into the model in future investigations.

3 Simulation Results

In this section, we present the results of simulations to steady state of the triad synapse.

The TRBDF2 (Bank et al. 1985; Gardner et al. 2004; Gardner and Jones 2011; Gardner et al. 2013) (trapezoidal rule-backward difference formula second-order) method is applied to the transport equations (6) and the ODEs (12). A parallelized version of the Chebyshev SOR method is used to solve Poisson's equation (7). The steady-state solutions in the figures are computed by simulating the time-dependent equations to steady state.

The background illumination is simulated by adjusting the potential U_{HC} inside the horizontal cell (see Fig. 2). As mentioned in the introduction, background illumination hyperpolarizes the horizontal cell. Thus, in all simulations, we use $U_{HC}^{off} = -40$ mV to simulate without background illumination and $U_{HC}^{on} = -60$ mV to simulate with background illumination. The bipolar cell intracellular potential is set to $U_{BC} = -60$ mV in Figs. 3–6. The fixed reference potential is held at $U_{ref} = -40$ mV for all simulations. The unknown biological parameters used for the calcium

channel model (13) are shown in Table 4. These parameters were tuned within a physiologically relevant range to get the best fit with the experimental calcium IV curve for goldfish (Fig. 11 of Verweij et al. (1996)) with background illumination off. Then the computed shifted calcium IV curve with an illuminated background is a *prediction* of our model.

In Figs. 3–6, we show color plots of the steady-state potential on a 600×900 grid, with and without background illumination, using several different values for U_{CP}. The color scale for the potential varies over different ranges in the figures in order to best portray the details of the potential variation, from -60 mV to $\{0, -20, -40, -40\}$ mV in Figs. 3–6, respectively. Note the hyperpolarization of the horizontal cell membrane potential and the depolarization of the cone pedicle membrane potential when the background is illuminated. To get a good view of the charge layers, we zoom in on the region containing the channels and plot the steady-state charge density as shown in Fig. 7. This figure verifies that the baths remain charge neutral away from the membranes and the charge layers that accumulate on each side are equal in magnitude but opposite in sign, i.e., the membrane also maintains overall neutrality.

We produced current-voltage curves in Figs. 8 and 9 with and without background illumination to observe how the model predicts the feedback response. The IV curves are generated by varying the cone pedicle holding potential U_{CP} over the range $[-80, 10]$ mV and then computing the calcium current I_{Ca} or hemichannel current I_{hemi} in steady state.

Good qualitative agreement is obtained between the computed (Fig. 8) and experimental (Fig. 11 in Verweij et al. (1996)) IV curves. Klaassen et al. (2011) present both experimental data on zebrafish and a theoretical argument that the shift in the calcium IV curve under background illumination is a pure translation, and that extraneous effects may have distorted the shift in Verweij et al. (1996)—our simulations here indicate a pure translation shift.

The hemichannel IV curves in Fig. 9 are just straight lines, as implied by the linear Ohm's law (14). Also note there is no experimental data on the hemichannel currents with which to compare.

The addition of the bipolar cell slightly complicates things. Some bipolar cells are known to depolarize under background illumination (OFF bipolar cells) and others are known to hyperpolarize under background illumination (ON bipolar cells). To understand how the intracellular potential of the bipolar cell affects the IV curves, we tried three different cases, which we label neutral, depolarized, and hyperpolarized. For all three cases, we use $U_{BC}^{off} = -60$ mV with no background illumination. When the background illumination is present, we use $U_{BC}^{on} = -60$ mV, -40 mV, and -80 mV for the neutral, depolarized, and hyperpolarized cases, respectively.

The bipolar cells are driven mainly by glutamate release from cones (and possibly are inhibited by GABA release from horizontal cells), so U_{BC} could in principle be derivable from an extension of the model. These effects will be investigated in future work.

Figures 8 and 9 show the results for all three cases along with the vertical shifts in the calcium and hemichannel IV curves. Figure 8 indicates that the shift in the calcium IV curves is enhanced when the bipolar cell

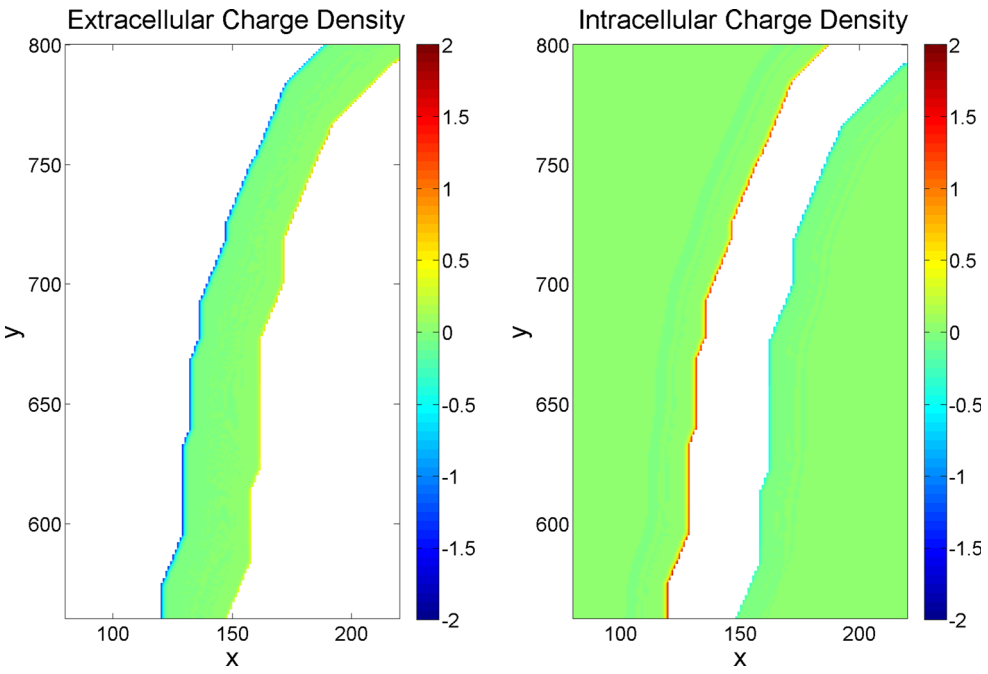

Fig. 7 A zoomed-in view of the steady-state charge density along the portion of the membranes containing ionic channels with $U_{CP} = -20$ mV, $U_{HC} = -40$ mV, and $U_{BC} = -60$ mV. Lengths are in nm and the charge density is in e·mM. Note that the charge layers on opposite sides of the membranes are equal in magnitude but opposite in sign

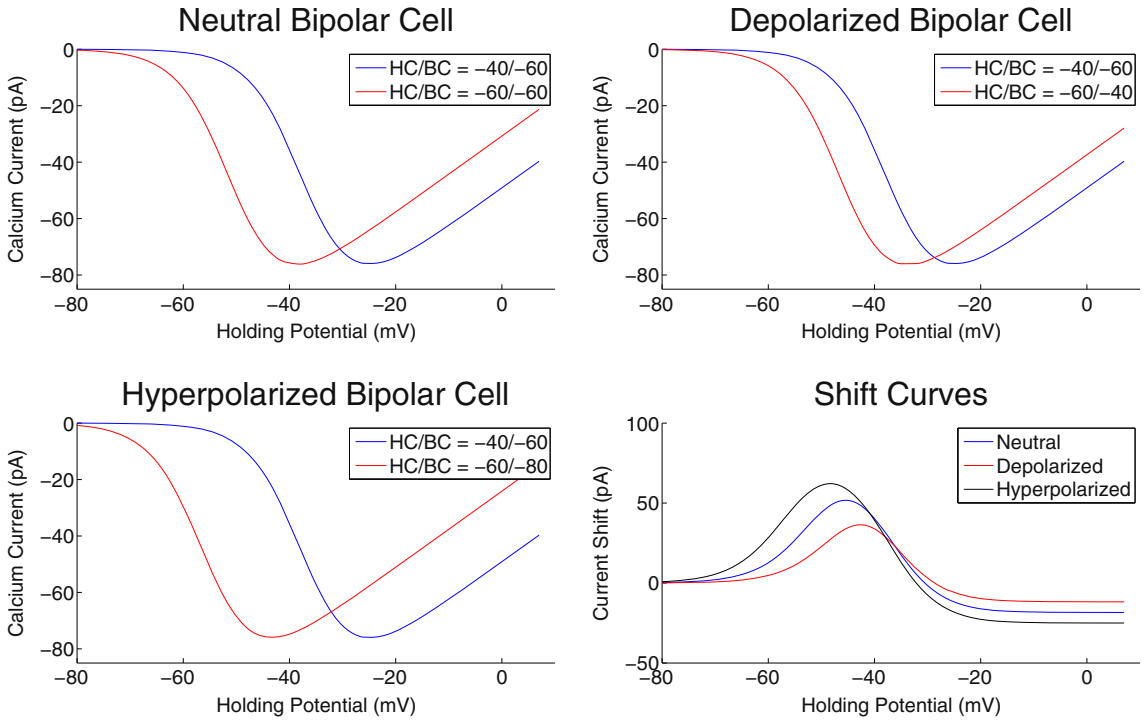

Fig. 8 Steady-state cone calcium transmembrane current-voltage curves (current or current shift in pA vs. cone pedicle holding potential in mV) for different bipolar cell intracellular potentials. *Top-left*: Neutral bipolar cell. *Top-right*: Depolarized bipolar cell. *Bottom-left*: Hyperpolarized bipolar cell. *Bottom-right*: Vertical difference of calcium IV curves for all three cases. Compare with Fig. 11 in Verweij et al. (1996)

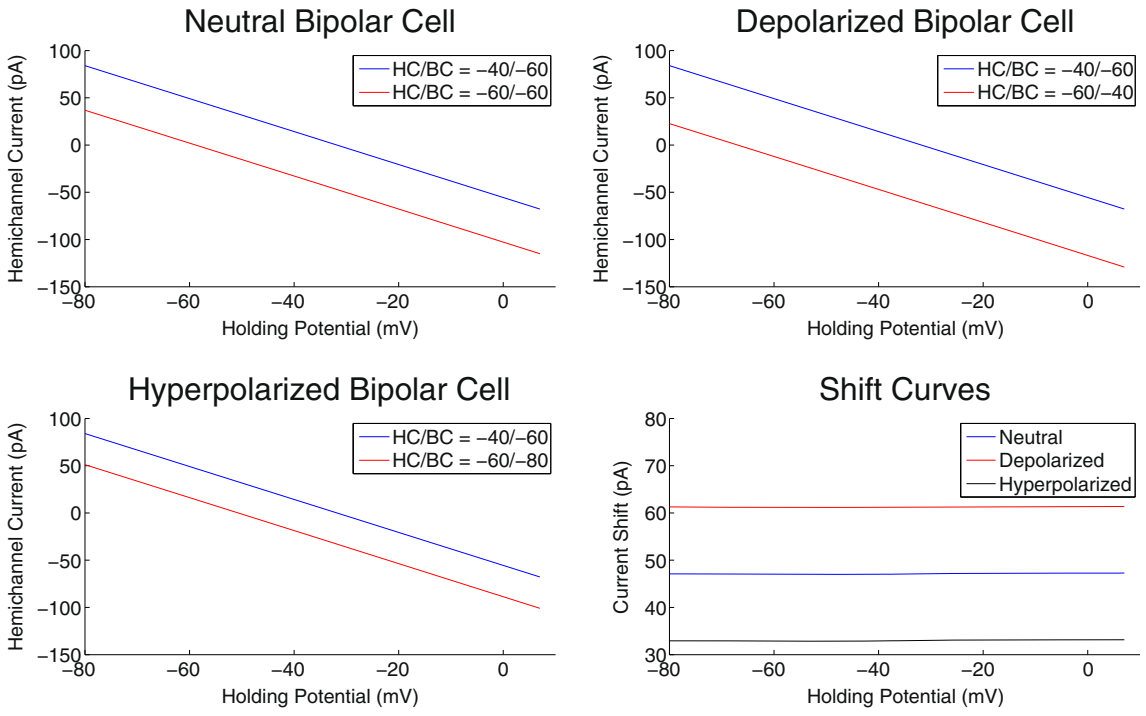

Fig. 9 Steady-state horizontal cell hemichannel transmembrane current-voltage curves (current or current shift in pA vs. cone pedicle holding potential in mV) for different bipolar cell intracellular potentials. Note that the hemichannel current can be either positive or negative, depending on the holding potential. *Top-left*: Neutral bipolar cell. *Top-right*: Depolarized bipolar cell. *Bottom-left*: Hyperpolarized bipolar cell. *Bottom-right*: Vertical difference of hemichannel IV curves for all three cases

is hyperpolarized and reduced when the bipolar cell is depolarized.

4 Conclusion

We have formulated a detailed spatial model of the triad synapse invaginating a cone pedicle in the outer plexiform layer of the retina. Our goal was to demonstrate the validity of the ephaptic hypothesis as a feedback mechanism. The results of our simulations have clearly verified that the ephaptic mechanism correctly shifts the calcium IV curve in the triad synapse when background illumination is applied. This shift was produced simply by hyperpolarizing the horizontal cell intracellular potential U_{HC}. Note that the feedback mechanism can be obtained by purely electrical effects only if there are high resistance pathways that electrically isolate the intersynaptic space.

As mentioned above, we obtained good qualitative agreement with the experimental calcium IV curves in Fig. 11 in Verweij et al. (1996). However our simulations support the contention of Klaassen et al. (2011) that both experimental data on zebrafish and a theoretical argument predict that the shift in the calcium IV curve under background illumination is a pure translation, and that extraneous effects may have distorted the shift in Verweij et al. (1996).

The simulations of the triad synapse also demonstrate the dependence of the feedback on the behavior of the bipolar cell under background illumination. The neutral case, shown in the upper left frame of Fig. 8 appears to be the closest match with the experimental data from Verweij et al. (1996). Since experiments measure currents for an entire cone pedicle with multiple triad synapses, our results suggest that there are approximately an equal number of ON and OFF bipolar cells in a given pedicle, which serve to balance out the shift effects. This result could be experimentally verified by blocking the ON bipolar cells with a chemical inhibitor, which would recover the contribution of the OFF biploar cells only.

Previous models of the feedback phenomena in the triad synapse have been compartment models in which each cell and the extracellular space are treated as isopotential regions (Byzov and Shura-Bura 1986; Dmitriev and Mangel 2006; Usui et al. 1996; Smith 1995). As illustrated in Figs. 3–6, our approach gives important information on the spatial variation in the potential within the cells of the synaptic circuit and the intersynaptic space. This information could facilitate the formulation of more detailed and accurate compartmental models of this or other complex invaginated synapses.

The feedback mechanism addressed in this paper is purely electrical. In Section 1.3 we discussed how the inhibitory neurotransmitter GABA may also be a candidate mechanism for feedback. In a multi-scale computational approach, Baer et al. (to appear) propose that GABA plays a secondary or modulatory role in the feedback with the ephaptic mechanism being dominant. In a future study we will test this hypothesis by investigating the GABA mechanism at the microscopic ionic level using the drift-diffusion model approach presented here.

Acknowledgments Research supported in part by the National Science Foundation under grant DMS-0718308. We thank Maarten Kamermans for valuable comments.

Conflict of interests The authors declare that they have no conflict of interest.

References

Ayoub, G.S., & Lam, D.M.K. (1985). The content and release of endogenous GABA in isolated horizontal cells of the goldfish retina. *Vision Research*, *25*(9), 1187–1193.

Babai, N., & Thoreson, W.B. (2009). Horizontal cell feedback regulates calcium currents and intracellular calcium levels in rod photoreceptors of salamander and mouse retina. *Journal of Physiology*, *587*(10), 2353–2364.

Baer, S.M., Chang, S., Crook, S.M., Gardner, C.L., Jones, J.R., Nelson, R.F., Ringhofer, C., Zela, D. (to appear). A computational study of background-induced flicker enhancement and feedback mechanisms in the vertebrate outer retina: temporal properties.

Bank, R.E., Coughran, W.M., Fichtner, W., Grosse, E.H., Rose, D.J., Smith, R.K. (1985). Transient simulation of silicon devices and circuits.

Barcilon, V., Cole, J., Eisenberg, R.S. (1971). A singular perturbation analysis of induced electric fields in nerve cells. *SIAM Journal on Applied Mathematics*, *21*, 339–354.

Barnes, S., Merchant, V., Mahmud, F. (1993). Modulation of transmission gain by protons at the photoreceptor output synapse. *Proceedings of the National Academy of Sciences of the United States of America*, *90*, 10081–10085.

Bouvier, M., Szatkowski, M., Amato, A., Attwell, D. (1992). The glial cell glutamate uptake carrier countertransports pH-changing anions. *Nature*, *360*, 471–474.

Byzov, A.L., & Shura-Bura, T.M. (1986). Electrical feedback mechanism in the processing of signals in the outer plexiform layer of the retina. *Vision Research*, *26*(1), 33–44.

Cadetti, L., & Thoreson, W.B. (2006). Feedback effects of horizontal cell membrane potential on cone calcium currents studied with simultaneous recordings. *Journal of Neurophysiology*, *95*, 1992–1995.

Chun, M., & Wässle, H. (1989). GABA-like immunoreactivity in the cat retina: Electron microscopy. *Journal of Comparative Neurology*, *279*(1), 55–67.

Davenport, C.M., Detwiler, P.B., Dacey, D.M. (2008). Effects of pH buffering on horizontal and ganglion cell light responses in primate retina: evidence for the proton hypothesis of surround formation. *Journal of Neuroscience*, *28*, 456–464.

DeVries, S.H. (2001). Exocytosed protons feedback to suppress the Ca^{2+} current in mammalian cone photoreceptors. *Nueronal*, *32*, 1107–1117.

Dmitriev, A.V., & Mangel, S.C. (2006). Electrical feedback in the code pedicle: a computational analysis. *Journal of Neurophysiology*, *95*, 1419–1427.

Dunlap, K., & Fischbach, G.D. (1981). Neurotransmitters decrease the calcium conductance activated by depolarization of embryonic chick sensory neurons. *Journal of Physiology—London*, *317*, 519–535.

Eisenberg, R.S. (1996). Computing the field in proteins and channels. *Journal of Membrane Biology*, *150*, 1–25.

Eisenberg, R.S., Klosek, M.M., Schuss, Z. (1995). Diffusion as a chemical reaction: stochastic trajectories between fixed concentrations. *Journal of Chemical Physics*, *102*, 1767–1780.

Eisenberg, B., Hyon, Y., Liu, C. (2010). Energy variational analysis EnVarA of ions in water and channels: field theory for primitive models of complex ionic fluids. *Journal of Chemical Physics*, *133*, 104104.

Fahrenfort, I., Steijaert, M., Sjoerdsma, T., Vickers, E., Ripps, H., et al. (2009). Hemichannel-mediated and pH-based feedback from horizontal cells to cones in the vertebrate retina. *PLoS ONE*, *4*(6), e6090.

Gardner, C.L., & Jones, J.R. (2011). Electrodiffusion model simulation of the potassium channel. *Journal of Theoretical Biology*, *291*, 10–13.

Gardner, C.L., Jones, J.R., Baer, S.M., Chang, S. (2013). Simulation of the ephaptic effect in the cone-horizontal cell synapse of the retina. *SIAM Journal on Applied Mathematics*, *73*, 636–648.

Gardner, C.L., Nonner, W., Eisenberg, R.S. (2004). Electrodiffusion model simulation of ionic channels: 1D simulations. *Journal of Computational Electronics*, *3*, 25–31.

Gerschenfeld, H.M., Piccolino, M., Neyton, J. (1980). Feed-back modulation of cone synapses by L-horizontal cells of turtle retina. *Journal of Experimental Biology*, *89*(0), 177–192.

Guo, C.Y., Hirano, A.A., Stella, S.L., Bitzer, M., Brecha, N.C. (2010). Guinea pig horizontal cells express GABA, the GABA-synthesizing enzyme GAD(65) and the GABA vesicular transporter. *Journal of Comparative Neurology*, *518*(1), 1647–1669.

Hirasawa, H., & Kaneko, A. (2003). pH changes in the invaginating synaptic cleft mediate feedback from horizontal cells to cone photoreceptors by modulating Ca^{2+} channels. *Journal of General Physiology*, *122*, 657–671.

Janssen-Beinhold, U., Schultz, K., Gellhaus, A., Schmidt, P., Ammermuller, J., Weiler, R. (2001). Identification and localization of connexin26 within the photoreceptor-horizontal cell synaptic complex. *Visual Neuroscience*, *18*, 169–178.

Johnson, M.A., & Vardi, N. (1998). Regional differences in GABA and GAD immunoreactivity in rabbit horizontal cells. *Visual Neuroscience*, *15*, 743–753.

Kamermans, M., & Fahrenfort, I. (2004). Ephaptic interactions within a chemical synapse: hemichannel-mediated ephaptic inhibition in the retina. *Current Opinion in Neurobiology*, *14*, 531–541.

Kamermans, M., Kraaij, D., Spekreijse, H. (2001). The dynamic characteristics of the feedback signal from horizontal cells to cones in the goldfish retina. *Journal of Physiology*, *534*(2), 489–500.

Kamermans, M., & Spekreijse, H. (1999). The feedback pathways from horizontal cells to cone: mini review with a look ahead. *Vision Research*, *39*, 2449–2468.

Klaassen, L.J., Sun, Z., Steijaert, M.N., Bolte, P., Fahrenfort, I., et al. (2011). Synaptic transmission from horizontal cells to cones is impaired by loss of connexin hemichannels. *PLoS Biology*, *9*(7), e1001107.

Lam, D.M.K., Lasater, E.M., Naka, K.-I. (1978). γ-aminobutyric acid: a neurotransmitter candidate for cone horizontal cells of the catfish retina. *Proceedings of the National Academy of Sciences of the United States of America*, *75*(12), 6310–6313.

Lam, D.M.K., Su, Y.Y.T., Swain, L., Marc, R.E., Brandon, C., Wu, J.-Y. (1979). Immunocytochemical localisation of L-glutamic acid decarboxylase in the goldfish retina. *Nature*, *278*(5), 565–567.

Mangel, S.C., Ariel, M., Dowling, J.E. (1985). Effects of acidic amino acid antagonists upon the spectral properties of carp horizontal cells: circuitry of the outer retina. *Journal Neuroscience*, *5*, 2839–2850.

Marc, R.E., Stell, W.K., Bok, D., Lam, D.M.K. (1978). GABA-ergic pathways in the goldfish retina. *Journal of Comparative Neurology*, *182*(2), 221–245.

Mori, Y., Jerome, J.W., Peskin, C.S. (2007). A three-dimensional model of cellular electrical activity. *Bulletin of the Institute of Mathematics Academia Sinica*, *2*, 367–390.

Mori, Y., & Peskin, C.S. (2009). A numerical method for cellular electrophysiology based on the electrodiffusion equations with internal boundary conditions at the membrane. *Communications in Applied Mathematics and Computational Sciences*, *4*, 85–134.

Mori, Y., Liu, C., Eisenberg, R.S. (2011). A model of electrodiffusion and osmotic water flow and its energetic structure. *Physica D: Nonlinear Phenomena*, *240*, 1835–1852.

Murakami, M., Shimoda, Y., Nakatani, K., Miyachi, E.I., Watanabe, S.I. (1982a). GABA-mediated negative feedback from horizontal cells to cones in carp retina. *Japanese Journal of Physiology*, *32*, 911–926.

Murakami, M., Shimoda, Y., Nakatani, K., Miyachi, E.I., Watanabe, S.I. (1982b). GABA-mediated negative feedback and color opponency in carp retina. *Japanese Journal of Physiology*, *32*, 927–935.

Nelson, R., Pflug, R., Baer, S.M. (1990). Background-induced flicker enhancement in cat retinal horizontal cells. II. spatial properties. *Journal of Neurophysiology*, *64*(2), 326–340.

Nonner, W., & Eisenberg, R.S. (1995). Ion permeation and glutamate residues linked by Poisson-Nernst-Planck theory in L-type calcium channels. *BioPhysical Journal*, *75*, 1767–1780.

Piccolino, M. (1995). The feedback synapse from horizontal cells to cone photoreceptors in the vertebrate retina. *Progress in Retinal and Eye Research*, *14*(1), 141–196.

Prodhom, B., Pietrobon, D., Hess, P. (1987). Direct measurement of proton transfer rates to a group controlling the dihydropyridine-sensitive Ca^{2+} channe. *Nature*, *329*, 243–246.

Schwartz, E.A. (1982). Calcium-independent release of GABA from isolated horizontal cells of the toad retina. *Journal of Physiology*, *323*, 211–227.

Schwartz, E.A. (1987). Depolarization without calcium can release gammaaminobutyric acid from a retinal neuron. *Science*, *238*(4825), 35–355.

Smith, R.G. (1995). Simulation of an anatomically defined local circuit: the cone-horizontal cell network in cat retina. *Visual Neuroscience*, *12*, 545–561.

Usui, S., Kamijama, Y., Ishii, H., Ikeno, H. (1996). Reconstruction of retinal horizontal cell responses by the ionic current model. *Vision Research*, *36*, 1711–1719.

Vardi, N., Kaufman, D.L., Sterling, P. (1994). Horizontal cells in cat and monkey retina express different isoforms of glutamic-acid decarboxylase. *Visual Neuroscience*, *11*(1), 135–142.

Verweij, J., Kamermans, M., Spekreijse, H. (1996). Horizontal cells feed back to cones by shifting the cone calcium-current activation range. *Vision Res.*, *36*(24), 3943–3953.

Vessey, J.P., Stratis, A.K., Daniels, B.A., Silva, N.D., Jonz, M.G., Lalonde, M.R., Baldridge, W.H., Barnes, S. (2005). Proton-mediated feedback inhibition of presynaptic calcium channels at the cone photoreceptor synapse. *The Journal of Neuroscience*, *25*(16), 4108–4117.